World Scientific
www.worldscientific.com

Multimodal Covariance Network Reflects Individual Cognitive Flexibility

Lin Jiang [*,†], Simon B. Eickhoff [‡,§], Sarah Genon [‡,§], Guangying Wang [*,†],
Chanlin Yi [*,†], Runyang He [*,†], Xunan Huang [†,¶], Dezhong Yao [*,†,‖,**],
Debo Dong [‡,††,‖‖,‡‡‡], Fali Li [*,†,‖,‡‡,***,‡‡‡] and Peng Xu [*,†,‖,§§,¶¶,†††,‡‡‡]

*The Clinical Hospital of Chengdu Brain Science Institute
MOE Key Lab for Neuroinformation, University of Electronic Science and
Technology of China, Chengdu 610054, P. R. China

†School of Life Science and Technology
Center for Information in Medicine
University of Electronic Science and Technology of China
Chengdu 611731, P. R. China

‡Institute of Neuroscience and Medicine
Brain and Behavior (INM-7), Research Center Jülich, Jülich, Germany

§Institute for Systems Neuroscience
Medical Faculty, Heinrich-Heine University Düsseldorf
Düsseldorf, Germany

¶School of Foreign Languages
University of Electronic Science and Technology of China
Sichuan, Chengdu 611731, P. R. China

‖Research Unit of NeuroInformation
Chinese Academy of Medical Sciences
2019RU035, Chengdu, P. R. China

**School of Electrical Engineering
Zhengzhou University, Zhengzhou 450001, P. R. China

††Faculty of Psychology, Southwest University
Chongqing 400715, P. R. China

‡‡Department of Electrical and Computer Engineering
Faculty of Science and Technology, University of Macau, Macau, P. R. China

§§Radiation Oncology Key Laboratory of Sichuan Province
ChengDu 610041, P. R. China

¶¶Rehabilitation Center, Qilu Hospital of Shandong University
Jinan 250012, P. R. China
‖‖debo.dong@gmail.com
***fali.li@uestc.edu.cn
†††xupeng@uestc.edu.cn

‡‡‡Corresponding authors.

Cognitive flexibility refers to the capacity to shift between patterns of mental function and relies on functional activity supported by anatomical structures. However, how the brain's structural–functional covarying is pre-configured in the resting state to facilitate cognitive flexibility under tasks remains unrevealed. Herein, we investigated the potential relationship between individual cognitive flexibility performance during the trail-making test (TMT) and structural–functional covariation of the large-scale multimodal covariance network (MCN) using magnetic resonance imaging (MRI) and electroencephalograph (EEG) datasets of 182 healthy participants. Results show that cognitive flexibility correlated significantly with the intra-subnetwork covariation of the visual network (VN) and somatomotor network (SMN) of MCN. Meanwhile, inter-subnetwork interactions across SMN and VN/default mode network/frontoparietal network (FPN), as well as across VN and ventral attention network (VAN)/dorsal attention network (DAN) were also found to be closely related to individual cognitive flexibility. After using resting-state MCN connectivity as representative features to train a multi-layer perceptron prediction model, we achieved a reliable prediction of individual cognitive flexibility performance. Collectively, this work offers new perspectives on the structural–functional coordination of cognitive flexibility and also provides neurobiological markers to predict individual cognitive flexibility.

Keywords: Cognitive flexibility; trail-making test; multimodal covariance network; EEG-MRI; response prediction.

1. Introduction

Cognitive flexibility, initially conceptualized by Coulson *et al.,*[1–3] has gradually evolved into a pivotal trait contributing to complicated tasks, e.g. providing adaptable solutions to varying needs, driving innovation, and promoting growth and discovery.[4] Individuals with high cognitive flexibility appear to be flexible enough to adapt to changing priorities and make use of unexpected opportunities. Hence, cognitive flexibility facilitates the recognition of novel semantic relations and the mellifluous generation of concepts and also reflects the adaptability of behavior and thought. Deficits in cognitive flexibility are usually seen in psychiatric illnesses including attention deficit hyperactivity disorder[5] and neuro-degenerative diseases including Parkinson's disease.[6] In children with autism, cognitive inflexibility is generally reported and is specifically linked with highly restricted and repetitive behaviors.[7] For adults, cognitive inflexibility is related to multiple clinical manifestations, e.g. symptom severity of post-traumatic stress disorder,[8] and among healthy older populations, cognitive flexibility decreases with age.[9]

Multiple strategies were proposed to assess human cognition,[10–12] with task-switching and set-shifting paradigms being commonly employed to measure individual cognitive flexibility. Thereinto,

the trail-making test (TMT) is a widely used neuropsychological tool that assesses the capacity to shift attention flexibly between competing task-set representations.[13] Two task components are included in the TMT, i.e. A and B. In TMT-A, participants are requested to connect circled numbers in sequential order using lines; while TMT-B requires participants to link circled numbers and letters alternately in ascending order (e.g. 1, A, 2, B, . . .). The task should be completed with utmost accuracy and efficiency by the participants, and the TMT performance is measured by the reaction time to accomplishment. As reported, the TMT has great potential for reflecting a broad range of cognitive functions including sequencing and shifting, visual search and scanning, attention, as well as the capacity to sustain subgoals synchronously.[14] Thereinto, the TMT B–A score (The difference in completion time between TMT-B and TMT-A) signifies a more reliable measurement of human cognitive flexibility, and a smaller TMT B–A score indicates higher cognitive flexibility.[15]

The evaluation of cognitive flexibility based on TMT relies greatly on the understanding and adaptability to the task designs for the tested individuals, which is relatively subjective. To overcome this shortcoming, as well as to mine the objective biomarkers, neural substrates underlying cognitive

flexibility have been studied either structurally or functionally. On one side, prefrontal white matter integrity,[16] and temporal cortex morphology[17] are essential for cognitive flexibility in healthy populations. Studies have documented that impairments in the white matter tracts of the left hemisphere, specifically within the superior arcuate/longitudinal fasciculus connecting parietal, temporal, and frontal cortices, are associated with a decline in cognitive flexibility.[18] On another side, the functional neuroimaging meta-analyses have further reported the distributed frontoparietal regions to participate in flexible switching, which consists of the high-level association cortex, occipital cortex, inferior temporal cortex, inferior and superior parietal cortices, and premotor cortex.[19,20] As a core system, the frontoparietal network (FPN) promotes the aggregation and regulation of neural activity that is extensively spread across the brain, thus establishing a coordinated framework for cognitive flexibility.[18]

In fact, human cognition is supported by inherent anatomical architectures with functional neural activity in the brain.[21] Both modalities are complementary and associated with each other, in particular, the structural framework shaping functional communication among different cerebral areas, leading to the emergence of various functional networks.[22] Hence, mapping the structural and functional coordination will deepen our understanding of how structural–functional covarying supports behavior and cognition, as well as provide new perspectives on comprehending the impact of diseases on the brain. Recently, to achieve the quantification of structural–functional coordination in the brain, a group-level multimodal covariance network (MCN)[23] was proposed to integrate functional magnetic resonance imaging (fMRI), diffusion magnetic resonance imaging (dMRI), structural magnetic resonance imaging (sMRI), and electroencephalograph (EEG) information simultaneously. Thereafter, individual MCN method[24] was further extended to detect functional neural co-activation within the inherent structural framework on an individual level. This strategy thereby allows us to investigate the structural–functional variation corresponding to inter-subject variability in human cognition. More importantly, individual MCN that integrate sMRI, dMRI, fMRI, and EEG modalities demonstrate the highest

sensitivity to reflect individual cognition and tracking disease severity in patients when compared to other covariance networks.[23] In particular, EEG provides an exceptional temporal resolution in the range of milliseconds, enables continuous monitoring and analysis of cognitive processes with fine-grained details, thus complementing the temporal aspect that is lacking in MRI imaging.[25,26]

Concerning cognitive flexibility, Medaglia and colleagues have shown that the alignment between the architecture of the white matter network and functional signals significantly relates to increased cognitive flexibility across individuals.[27] Namely, both structural and functional variations, particularly the combined features of functional processes and anatomical organization, are of great significance for understanding cognitive flexibility. However, the structural–functional pre-configurations supporting cognitive flexibility are still unrevealed. Hence, by adopting large-scale MCN, the relationships between baseline structural–functional configurations and individual TMT B–A scores were probed from three levels (i.e. network topology, whole-brain network properties, and subnetwork properties). Based on this, related MCN predictors were uncovered, with a multi-layer perceptron prediction model being built to help predict individual TMT performance. Finally, potential MCN differences between individuals with varying cognitive flexibility were revealed.

2. Methods

2.1. *Participants*

Herein, a total of 182 unmedicated healthy participants (63 females, aged 20–80 years) were enrolled with the approval of the ethics committee at the medical faculty of the University of Leipzig. All participants willingly gave their written informed consent. The multimodal brain data and cognitive tests were acquired from the Functional Connectomes Project International Neuroimaging Data-Sharing Initiative http://doi.org/10.15387/fcp_indi.mpi_lemon (2018).[28] Participants were excluded due to significant movement of the head (rotation $> 3.0°$ or translation > 3.0 mm) in resting-state fMRI collection or artifacts in EEG signals, as well as those who did not have complete multimodal brain imaging, EEG,

and cognitive tests. Finally, 161 participants were reserved in the following analysis.

2.2. *TMT*

To measure individual cognitive flexibility, participants were asked to perform the TMT task, which consisted of parts A and B.[29] In TMT-A, individuals are instructed to connect 25 numbered circles on a sheet of paper in sequential order (e.g. 1, 2, 3, etc.); whereas in TMT-B, individuals must link numbered and lettered circles in an alternating sequence (e.g. 1, A, 2, B, etc.). The performance of each subtest is represented by the duration used to accomplish the task, and the TMT B–A score, which is computed by subtracting the completion time of TMT-B from that of TMT-A, representing an objective and valid measure for cognitive flexibility.

2.3. *Multimodal data acquisition and preprocessing*

In this study, a 3 Tesla scanner (MAGNETOM Verio, Siemens Healthcare GmbH, Erlangen, Germany) with a 32-channel head coil was utilized to record the MRI. EEG was collected by a BrainAmp MR plus amplifier equipped with 62-channel active ActiCAP electrodes (Brain Products GmbH, Gilching, Germany). More details about data recording can be found in Ref. 28.

The dMRI preprocessing was performed using the FMRIB Software Library (FSL).[30] package. We first conducted a thorough evaluation of data quality by iteratively examining each image, aiming to identify gross artifacts including interleave artifacts and signal dropouts resulting from abrupt participant movement. Next, the FMRIB Diffusion Toolbox was utilized to correct participant motion effect and eddy current-induced distortion. The first B0 image was utilized for generating the brain mask using the brain extraction tool, while a linear least-squares fitting technique was employed for estimating the diffusion tensor model.

Meanwhile, following the preprocessing pipeline at https://github.com/NeuroanatomyAndConnectivity/ pipelines/tree/master/src/lsd_lemon,[31] the CBS tools were first used to eliminate the background of the uniform T1-weighted image.[32] Then, cortical surface reconstruction was applied to the masked image by recon-all in FreeSurfer,[33,34] based on which brain

mask was produced. Finally, to achieve the registration between individual T1-weighted images and Montreal Neurological Institute (MNI) 152 standard space, a nonlinear transformation algorithm named Symmetric Normalization[35] in the Advanced Neuroimaging Tools software was performed. This strategy maximizes the cross-correlation within the space of diffeomorphic maps and provides the Euler–Lagrange equations necessary for this optimization, thereby achieving a balanced trade-off between speed, flexibility, and performance.[36]

The fMRI preprocessing was conducted using the Data Processing & Analysis of Brain Imaging (DPABI; http://rfmri.org/DPABI) toolkit. Specifically, the first 10 volumes were eliminated and the remaining ones were reserved to correct variances in time and movement of the head. Afterward, images underwent spatial normalization to fit the standard MNI space. Subsequently, they were resliced with a resolution of $2 \times 2 \times 2\,\text{mm}^3$ and subjected to spatial smoothing (6 mm full-width at half-maximum [FWHM]). Additionally, a band-pass filter was applied within the frequency range of 0.01–0.1 Hz. Ultimately, we regress the averaged cerebrospinal fluid signal, white matter signal, and 24 parameters obtained through the rigid-body head motion correction.

For EEG, we initially re-referenced the raw EEG using the reference electrode standardization technique (REST).[37] To eliminate any ocular artifacts, we applied independent component analysis (ICA),[38] and then performed offline bandpass filtering within the frequency range of 1–30 Hz. Subsequently, we conducted data segmentation into 10 s intervals and removed any artifacts exceeding $\pm 100\,\mu\text{V}$. To align with the high spatial resolution of MRI and match the head model accurately, we employed standardized low-resolution electromagnetic tomography (sLORETA)[39] for reconstructing cortical source activity.

2.4. *Constructing the MCN*

According to the Desikan–Killiany (DK) atlas, we divided the cortical surface into 308 regions-of-interest (ROIs).[40] We expanded and interpolated the parcellated DK atlas to match the respective fMRI, dMRI, and EEG source space.[40] Owing to the disparities between the head model of EEG source space and MRI, a total of 303 brain areas were successfully

Table 1.   The unmatched and discarded regions of the DK atlas.

| ROI | MNI | | | Structural name |
	X	Y	Z	
1	−39.72	11.34	48.85	lh_caudalmiddlefrontal_part4
1	−48.10	30.82	5.23	lh_parstriangularis_part1
3	−40.49	31.11	−0.50	lh_parstriangularis_part2
4	−35.45	4.28	−0.59	lh_insula_part4
5	23.85	−65.16	38.59	rh_superiorparietal_part5

aligned and subsequently incorporated in the subsequent procedures. See Table 1 for those excluded areas.

As previously proved, in comparison with covariance networks constructed by MRI or EEG alone, or the pairwise combination of structural, functional MRI, and EEG features, MCN that integrates structural–functional-EEG modalities has higher replicability in detecting the brain's structural–functional covarying, exhibiting the highest sensitivity to reflect individual cognition and to track the disease severity of depression patients.[24] Therefore, following the previous study,[24] multimodal features were calculated based on sMRI, dMRI, fMRI, and EEG datasets.

First, given that structural properties of the human cortex can be more precisely estimated by combined analysis of more than one MRI morphometric index,[41–43] multiple cortical structural features were combined in a single participant. Thereinto, dMRI provides an indirect assessment of the myeloarchitecture in various brain regions. Two commonly concerned dMRI features including the mean diffusivity representing the rotationally invariant magnitude of water diffusion within brain tissue, and the fractional anisotropy measuring the level of anisotropy of water diffusion within tissues,[44] were calculated. In terms of the sMRI which assesses macroscopic morphology of the cortex, seven commonly used morphological features including cortical thickness, curvature index, surface area, mean curvature, Gaussian curvature, gray matter volume, and folding index were calculated. Thereinto, the gray matter volume was obtained by calculating the average values across all voxels in the regions; cortical thickness was determined as the mean distance

between the pial surface and white surface; while the calculation of surface area involved determining the area of the intermediate layer situated between the surfaces of gray matter and white matter. Besides, the inverse of the radius of the circle that touches the surface at each vertex of a triangle was used to estimate the curvature index; the product of the principal curvatures defines Gaussian curvature, while mean curvature is defined as the average of two principal curvatures (1/radius of an inscribed circle).[45,46]

Meanwhile, it is extensively documented that functional and structural modalities exhibit a complementary relationship, with each modality typically capturing distinct aspects of brain function or structure.[22] Hence, following the same strategy, multiple functional features were also calculated from fMRI and EEG. In terms of fMRI, which assesses the hemodynamic response related to the brain's neural activity, the amplitude of low-frequency fluctuation, fractional amplitude of low-frequency fluctuations, and regional homogeneity were computed as the average values across all voxels within each region.

Theoretically, the amplitude of low-frequency fluctuation is computed as the average square root of the power spectrum in a low-frequency band and can detect the characteristics of the most dominant frequency component of the resting state.[47] In theory, the amplitude of low-frequency fluctuation is determined by calculating the average square root of the power spectrum within a specific range of low frequencies and can identify the features of the most dominant frequency component during rest.[47] In addition, the fractional amplitude of low-frequency fluctuations is determined by dividing the total power of the low-frequency range by the overall power across all frequencies; while regional homogeneity measures the resemblance between the time series of individual voxel and those of their adjacent voxels, thus providing a valuable technique for examining local brain activity.[48] Regarding the EEG, which provides insights into the intricate temporal patterns of neural electrical activity,[49] we initially extracted time series for each ROI. To evaluate the functional connections among various brain regions, we employed the phase-locking value as a metric to quantify the inter-regional synchronization of source

EEG signals. Given that crucial brain regions can promote functional integration and play a critical role in network resilience to damage, centrality measures that assess the significance of individual nodes are considered as EEG features.[50] Thereinto, the degree centrality of node i is determined by the cumulative number of edges it is connected to. Nodes with higher degree centrality demonstrate extensive functional associations with multiple other nodes in the network.

$$\text{DC}_i = \sum_{j=1}^{N} w_{ij}. \tag{1}$$

The closeness centrality can be mathematically expressed as the reciprocal of the mean shortest distance between a specific node and all other nodes in the network.

$$\text{CC}_i = \frac{n-1}{\sum\limits_{j \in N, j \neq i} d_{ij}}. \tag{2}$$

Betweenness centrality is defined as the proportion of all shortest paths in a network that traverses through a specific node.

$$\text{BC}_i = \frac{1}{(n-1)(n-2)} \sum_{\substack{h, j \in N \\ h \neq j, h \neq i, j \neq i}} \frac{\rho_{hi}(i)}{\rho_{hi}}. \tag{3}$$

Meanwhile, eigenvector centrality is the first eigenvector of the adjacency matrix, corresponding to the largest eigenvalue λ_1 (i.e. principal eigenvalue).

$$EC_i = \frac{1}{\lambda_1} \sum_{j=1}^{N} w_{ij} \mu_1(j), \tag{4}$$

where N is the number of nodes in the network. w_{ij} and d_{ij} denote the edge and shortest path length between node i and node j. ρ_{hj} indicates the number of shortest paths between h and j, and $\rho_{hj}(i)$ is the number of shortest paths between h and j that pass through i. $\mu_1(j)$ denotes the jth component of the first eigenvector of the adjacency matrix.

Then, functional and morphometric features were concatenated as a vector and then z-normalized, and Pearson's correlation analysis was conducted between pairwise ROIs, resulting in 303×303 adjacent matrices per subject. Therefore, the $\text{MCN} \in R^{303 \times 303}$

can be computed based on 303 ROIs of the DK atlas as

$$\text{MCN} = \begin{bmatrix} w_{1,1}^{PCC} & w_{1,2}^{PCC} & \cdots & w_{1,303}^{PCC} \\ w_{2,1}^{PCC} & w_{2,2}^{PCC} & \cdots & w_{2,303}^{PCC} \\ \vdots & \vdots & \cdots & \vdots \\ w_{303,1}^{PCC} & w_{303,2}^{PCC} & \cdots & w_{303,303}^{PCC} \end{bmatrix}, \tag{5}$$

where $w_{i,j}^{PCC}$ is Pearson's correlation coefficient between roi_i and roi_j.

2.5. *Network properties*

Graph theory is increasingly applied as a reliable tool for determining the properties of brain networks.[51,52] After constructing MCN for each participant, four network properties, i.e. characteristic path length (L), global efficiency (Ge), local efficiency (Le), and clustering coefficient (C), were calculated by the brain connectivity toolbox to quantify the potential for functional segregation and integration of the brain.[50] Therein, the potential for functional integration is reflected by L and Ge, while the potential for functional segregation between brain lobes is indicated by Le and C. Specifically, L is determined by calculating the average shortest distance between every pair of nodes in the network; Ge represents the mean efficiency of the corresponding brain network; Le denotes the average efficiency of local subgraphs; and C is defined as the proportion of triangles surrounding an individual node in the network.

$$L = \frac{1}{N} \sum_{i \in \theta} L_i = \frac{1}{N} \sum_{i \in \theta} \frac{\sum\limits_{j \in \theta, j \neq i} d_{ij}}{N-1}, \tag{6}$$

$$\text{Ge} = \frac{1}{N} \sum_{i \in \theta} \frac{\sum\limits_{j \in \theta, j \neq i} d_{ij}^{-1}}{N-1}, \tag{7}$$

$$\text{Le} = \frac{1}{N} \sum_{i \in \theta} \frac{\sum\limits_{j,l \in \theta, j \neq i} (C_{ij} C_{il} [d_{jl}(\theta_i)]^{-1})^{1/3}}{\sum\limits_{j \in \theta} C_{ij} (\sum\limits_{j \in \theta} C_{ij} - 1)}, \tag{8}$$

$$C = \frac{1}{N} \sum_{i \in \theta} \frac{\sum\limits_{j,l \in \theta} (w_{ij} w_{il} w_{jl})^{1/3}}{\sum\limits_{j \in \theta} w_{ij} (\sum\limits_{j \in \theta} w_{ij} - 1)}, \tag{9}$$

where d_{ij} and w_{ij} indicate the weighted shortest path length and the weighted connectivity strength

between nodes i and j, respectively. N and θ denote the number of nodes and the set of all network nodes, respectively.

2.6. *Statistical analysis*

Herein, Pearson's correlations with a false discovery rate (FDR) correction were first employed to explore the underlying relationships between the TMT B–A scores and resting-state MCN topology, brain-wide MCN properties, and subnetwork properties. In addition, following the protocol used in previous studies,[53,54] all participants were divided into two groups based on their TMT B–A scores. Concretely, participants having large TMT B–A scores were assigned to the low flexibility group, by contrast, those who had small TMT B–A scores were assigned to the high flexibility group. Thereafter, independent-sample t-tests were used to evaluate the differences in TMT performance/MCN topology/network properties between the low- and high-flexibility groups. These results would be further corrected for multiple testing by the FDR.

2.7. *Prediction of the TMT scores*

To further verify the relationship between MCN and cognitive flexibility, a multi-layer perceptron model was built to predict individual TMT B–A scores, adopting multiple MCN features that have significant correlations with TMT B–A scores. Specifically, we designed a simple multi-layer perceptron with two hidden layers containing 32 and 16 neurons, respectively. Dropouts were included in the two layers to impart robustness in the learning process and prevent overfitting, with a dropout ratio of 0.25. Adam algorithm with a learning rate of 0.01 was used for optimization.[55]

Herein, a ten-fold cross-validation strategy was performed to evaluate the prediction performance, along with the Pearson's correlation coefficients between the actual and predicted TMT B–A scores, root mean square error (RMSE),[56] and R^2[57] were calculated to quantify the prediction error. As proved, the R^2 exhibits negative values when the regression performs poorly, while it ranges between 0 and 1 (inclusive) to indicate a good regression performance.[57] A positive value of R^2 can be considered similar to the percentage of correctness obtained by the regression.

$$\text{RMSE} = \sqrt{\frac{1}{n}\sum_{i=1}^{n}(x_i - y_i)^2}, \qquad (10)$$

$$R^2 = 1 - \frac{\sum_{i=1}^{n}(x_i - y_i)^2}{\sum_{i=1}^{n}(\bar{y} - y_i)^2}, \qquad (11)$$

where n denotes the number of participants. y_i and x_i indicate the actual and predicted TMT B–A scores, respectively. $\bar{y}$ is the mean actual TMT B–A scores.

3. Results

3.1. *Study overview*

Herein, based on multimodal neuroimaging and EEG datasets, large-scale MCN was constructed to quantify the structural–functional coordination and to probe its relationship with individual cognitive flexibility. Given the breadth of cognitive requirements underlying cognitive flexibility, it is plausible to consider that cognitive flexibility may rely on multitudinous functional subsystems rather than originating from a single cognitive "module".[58] As such, by setting large-scale functional subnetworks as modules and the connectivity among module nodes as edges, we can quantitatively evaluate the structural–functional interactions within and across subnetworks, which form the MCN to reveal the structural–functional pre-configurations supporting cognitive flexibility at a large-scale level. To achieve this, all ROIs were allocated to functional subnetworks within the Yeo 7 framework,[59] which encompasses the FPN, somatomotor network (SMN), visual network (VN), default mode network (DMN), limbic network (LN), ventral attention network (VAN), and dorsal attention network (DAN). Then, the relationship between MCN topology/properties and TMT B–A scores was probed, and a multi-layer perceptron prediction model was established to predict TMT performances for all participants. Finally, MCN topology and properties differences between people with high and low flexibility were further uncovered.

3.2. *MCN correlated with individual cognitive flexibility*

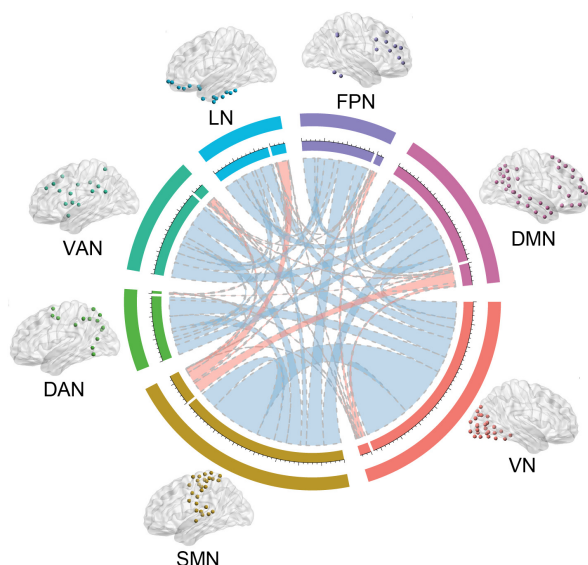On the one hand, when probing the relationship between resting-state MCN topology and TMT B–A

Fig. 1. (Color online) MCN topologies significantly correlated with TMT B–A scores ($p_{\text{FDR}} < 0.01$). The blue and red solid lines represent edges with significantly negative and positive correlations with TMT B–A scores, respectively.

scores, strong inter-subsystem interactions specifically distributed in the SMN and VN/FPN/DMN, as well as intra-subsystem connectivity in the SMN and VN, were identified to be significantly negatively related to individual TMT B–A scores ($p_{\text{FDR}} < 0.01$; Fig. 1). In the meantime, for each participant, four quantified properties, e.g. Le, Ge, L, and C of both brain-wide MCN and corresponding subnetworks were calculated.[50] We then correlated the network properties at the individual level with TMT B–A scores, to mine the significant relationship between the two concerned variables. Figure 2 shows that the Le ($r_{(159)} = -0.28$, $p_{\text{FDR}} < 0.01$), Ge ($r_{(159)} = -0.32$, $p_{\text{FDR}} < 0.01$), and C ($r_{(159)} = -0.28$, $p_{\text{FDR}} < 0.01$) of the brain-wide MCN were significantly negatively correlated with TMT B–A scores, and L was significantly positively associated with TMT B–A scores ($r_{(159)} = 0.38$, $p_{\text{FDR}} < 0.01$).

Further, among the YEO seven subsystems, the TMT B–A scores showed a significant negative relation with the Le, Ge, and C of the SMN, VAN, and
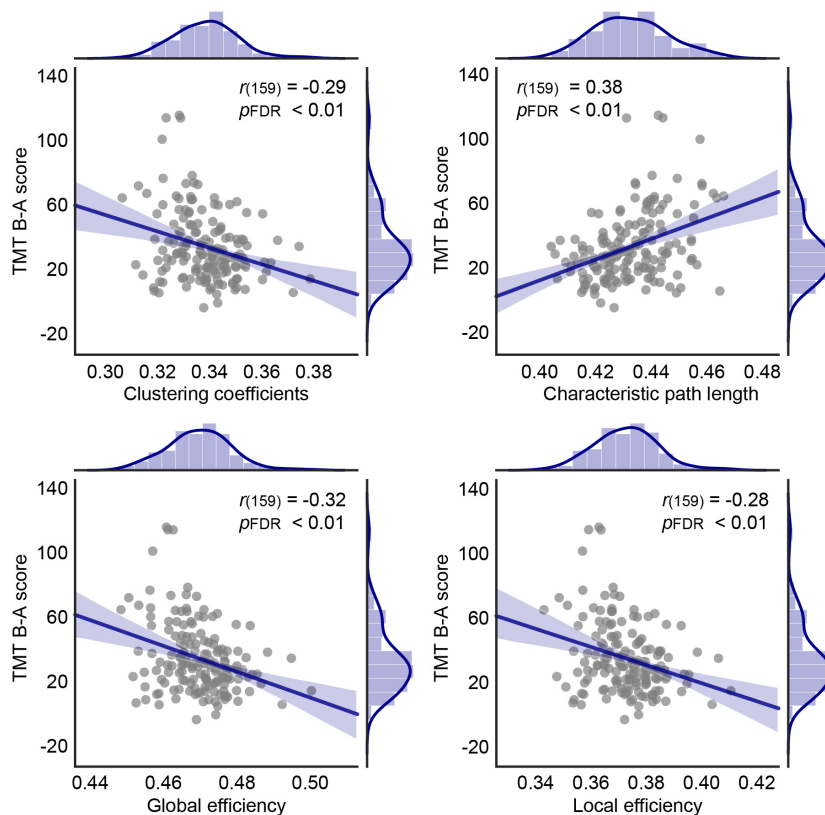

Fig. 2. (Color online) Correlation between brain-wide MCN properties and TMT B–A scores. In each subfigure, the purple line indicates the fitted curve, r is the correlation coefficient, and p is the statistical significance level.

VN. Conversely, there was a positive relation between the TMT B–A scores and the L of the SMN, VAN, and VN ($p_{\mathrm{FDR}} < 0.05$; Fig. 3; the detailed r- and p-values are shown in Table 2).

3.3. *Differential MCN between low- and high-flexibility populations*

As illustrated previously, a smaller TMT B–A difference corresponds to higher cognitive flexibility. The negative correlations between TMT B–A scores and MCN topology/properties suggested that participants with higher cognitive flexibility (i.e. smaller TMT B–A scores) may have both stronger structural–functional connectivity and larger network

properties. To further validate this, following the protocol used in previous studies,[53,54] participants were divided into two groups based on their TMT B–A scores, namely, the low and high flexibility groups, to explore the underlying MCN differences. Figure 4(a) exhibits that, the TMT B–A scores of the low flexibility group were significantly higher than that of the high flexibility group ($t_{(159)} = 13.61$, $p < 0.001$). The differential MCN topology shown in Fig. 4(b) demonstrated notably enhanced intra-subsystem connections within the VN and SMN, as well as enhanced inter-subsystem linkages spanning across the VN and SMN/VAN/DAN, among participants with higher levels of flexibility compared to those with lower levels ($p_{\mathrm{FDR}} < 0.01$). And a small

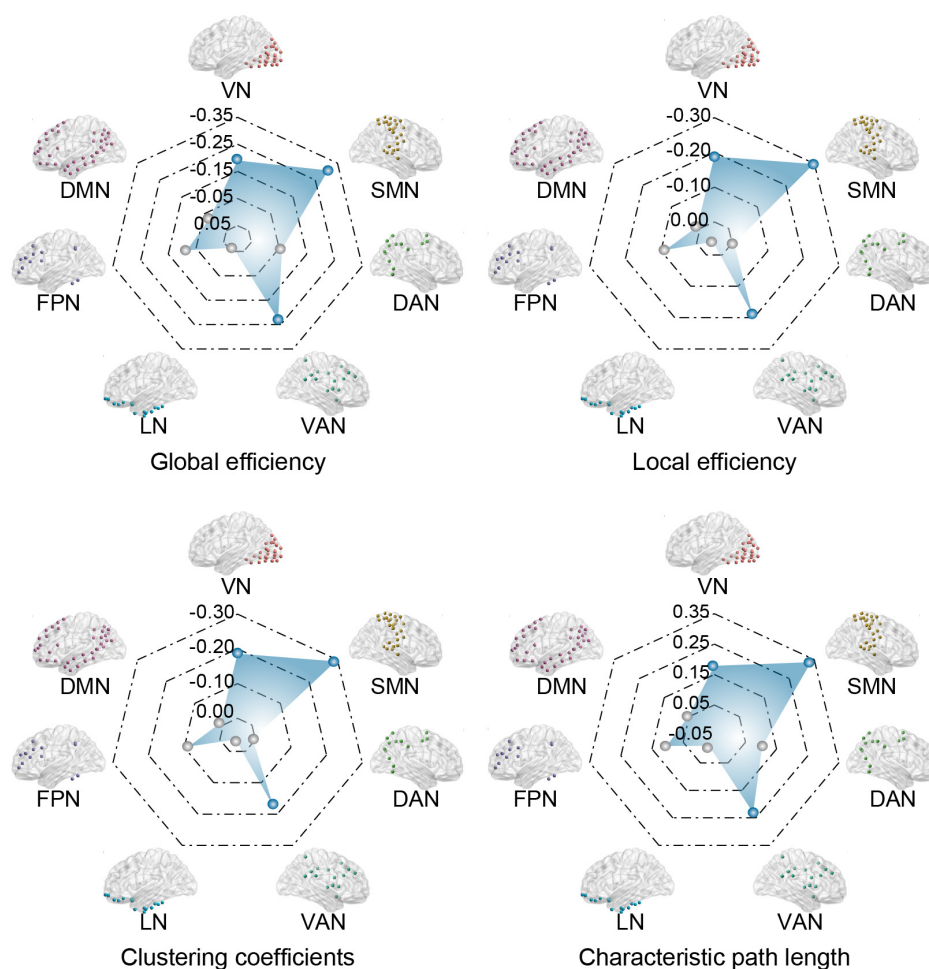Fig. 3. (Color online) Correlation between subnetwork properties and TMT B–A scores. The radar map shows the correlation coefficient between the properties of each subnetwork and TMT B–A scores. The small circles in the radar map show the specific correlation coefficients, and the blue circles denote subnetworks with significantly positive or negative correlations with TMT B–A scores ($p_{\mathrm{FDR}} < 0.05$).

Table 2. Pearson's correlations between subnetwork properties and individual TMT B–A scores ($n = 161$).

		VN*	SMN*	DAN	VAN*	LN	FPN	DMN
Le	R	−0.19	−0.30	−0.01	−0.19	0.04	−0.09	−0.01
	p_{FDR}	0.02	0.00	0.95	0.02	0.60	0.28	0.91
Ge	R	−0.19	−0.31	−0.06	−0.23	0.06	−0.08	−0.02
	p_{FDR}	0.02	0.00	0.45	0.00	0.42	0.30	0.76
L	R	0.18	0.34	0.10	0.23	−0.01	0.10	0.05
	p_{FDR}	0.02	0.00	0.19	0.00	0.88	0.20	0.51
C	R	−0.19	−0.29	0.01	−0.17	0.04	−0.09	−0.01
	p_{FDR}	0.02	0.00	0.92	0.03	0.64	0.28	0.91

Notes: * indicates the significant Pearson's correlations between subnetwork properties and individual TMT B–A scores. r is the correlation coefficient, and p is the statistical significance level. Le — local efficiency, Ge — global efficiency, L — characteristic path, C — clustering coefficients.
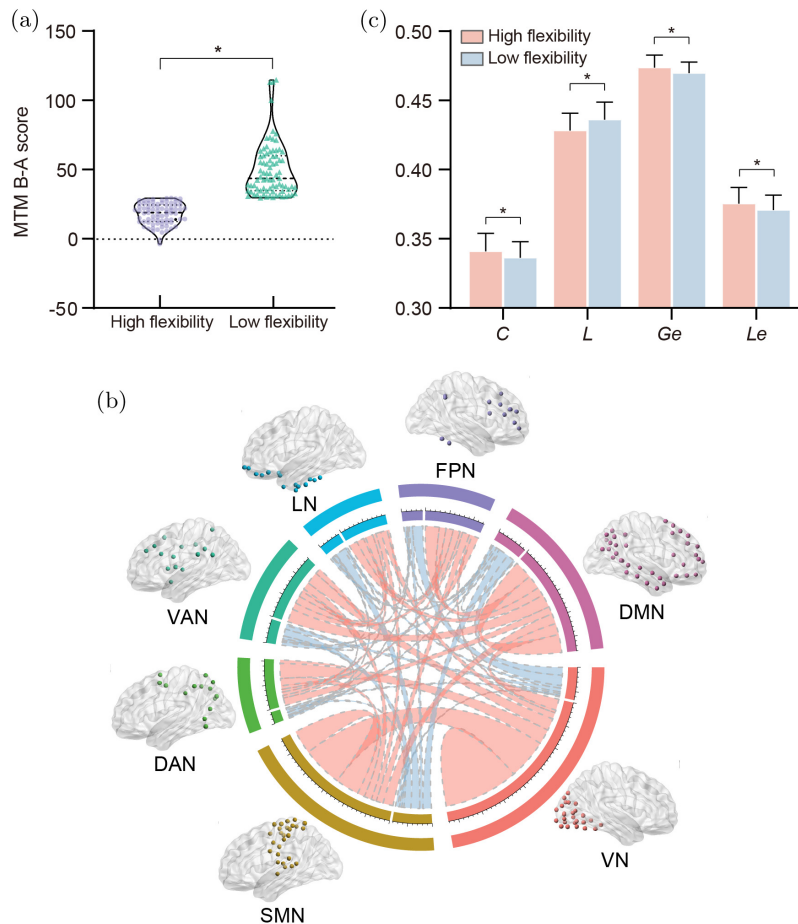

Fig. 4. (Color online) Differential MCN between high and low flexibility groups. (a) The TMT B–A scores of high and low flexibility groups. The purple and green violin plot shows the TMT B–A scores of the high and low flexibility groups, respectively. * represents $p < 0.01$. (b) Differences in MCN topologies between the two groups ($p_{FDR} < 0.01$). The blue and red solid lines denote the significantly weaker and stronger MCN connectivity of the high flexibility group compared to those of the low flexibility group, respectively. (c) Differences in brain-wide MCN properties between the two groups. *represents $p_{FDR} < 0.05$.

proportion of weaker inter-subsystem connections between the SMN and VAN/LN/DMN were observed in the high flexibility group ($p_{FDR} < 0.01$), as well. In line with the MCN differences in Fig. 4(b), network properties of the brain-wide MCN in the high flexibility group were demonstrated to be significantly greater than that of the low flexibility one (Le: $t_{(159)} = 2.55$, $p_{FDR} < 0.01$; Ge: $t_{(159)} = 2.93$, $p_{FDR} < 0.01$; L: $t_{(159)} = -3.90$, $p_{FDR} < 0.01$; C: $t_{(159)} = 2.45$, $p_{FDR} < 0.01$; Fig. 4(c)). More interestingly, referring to the subsystems in Fig. 5, in contrast to the low flexibility participants, high flexibility individuals showed significantly increased properties mainly in the VN and SMN ($p_{FDR} < 0.05$; The detailed t- and p-values are shown in Table 3).

3.4. *TMT performance prediction*

Considering the close correlations between MCN and TMT B–A scores, MCN features could potentially enhance the ability to predict an individual's cognitive flexibility, e.g. the TMT B–A scores.

Accordingly, based on network features that have significant correlations with TMT B–A scores, a multi-layer perceptron model was employed to achieve the prediction of the TMT performance. Herein, the ten-fold cross-validation strategy was performed. Figure 6 illustrates the correlation between predicted and actual TMT B–A scores. Our findings demonstrate that MCN features significantly contribute to predicting TMT B–A scores ($r = 0.67$, $p < 0.001$), with the RMSE calculated as 16.19, and R^2 as 0.44.

4. Discussion

Herein, we probed the relationship between the TMT performance and resting-state MCN of healthy participants, to uncover the preconfigured structural–functional substrates supporting human cognitive flexibility. After constructing the MCN for all participants, we primarily correlated the TMT B–A performance with individual MCNs at three levels including the large-scale MCN topology, whole-brain
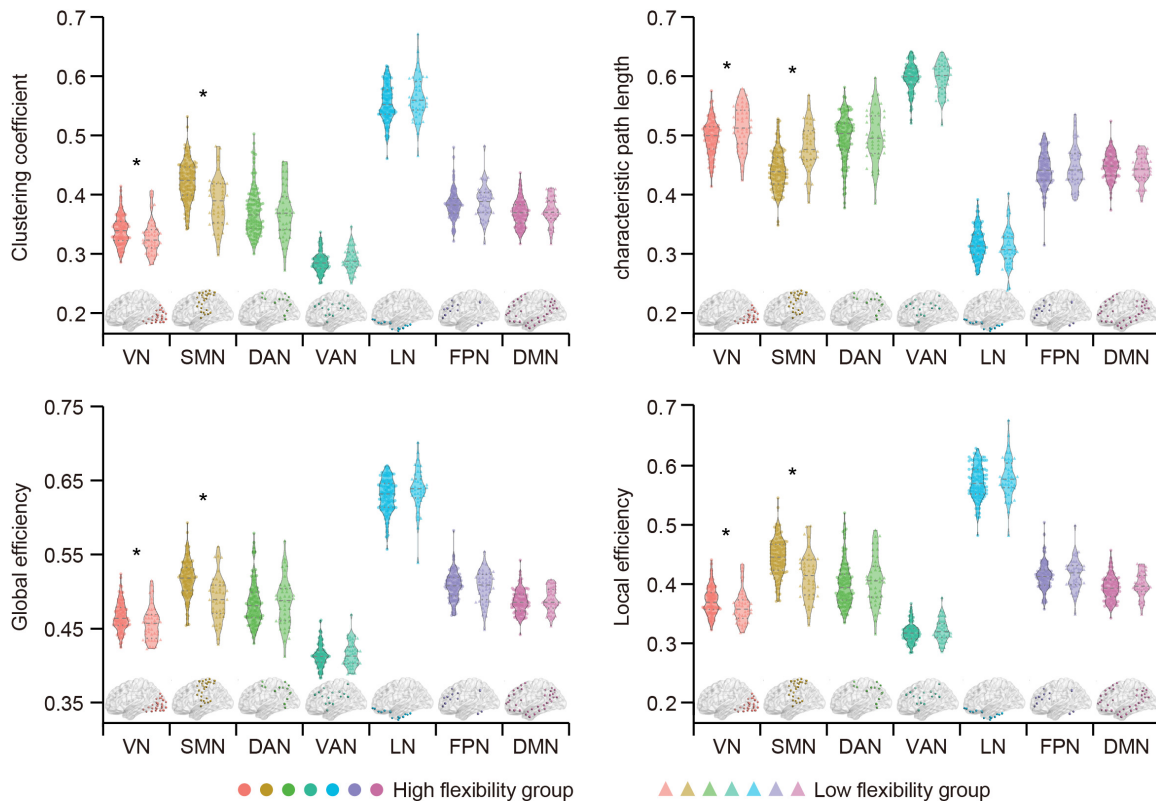

Fig. 5. Differences in subnetwork properties between high and low flexibility groups. *represents $p_{FDR} < 0.05$.

Table 3. Statistical differences (t- and p-values) between participants in the high and low flexibility groups.

		VN*	SMN*	DAN	VAN	LN	FPN	DMN
Le	t	1.98	1.77	−0.36	0.34	−0.43	0.29	−0.48
	$p_{\rm FDR}$	0.03	0.04	0.64	0.37	0.67	0.39	0.68
Ge	t	2.29	1.86	0.16	0.55	−0.49	0.22	−0.36
	$p_{\rm FDR}$	0.01	0.03	0.44	0.29	0.69	0.41	0.64
L	t	−2.69	−2.03	−0.51	−0.59	−0.15	−0.42	0.35
	$p_{\rm FDR}$	0.00	0.00	0.30	0.28	0.44	0.34	0.64
C	t	1.89	1.74	−0.49	0.24	−0.44	0.28	−0.46
	$p_{\rm FDR}$	0.03	0.04	0.69	0.41	0.67	0.39	0.68

Notes: * indicates the significant differences in subsystem properties between the two groups. Le — local efficiency, Ge — global efficiency, L — characteristic path, C — clustering coefficients.

network properties, and subsystem properties. As identified, the intra-subsystem covariation of the SMN and VN and inter-subsystem covariation spanning the SMN and VN/FPN/DMN, are significantly related to individual TMT B–A scores. Meanwhile, significant correlations were observed between the TMT B–A scores and both the whole-brain MCN properties and subsystem properties (particularly the SMN and VN). When further investigating the potential MCN differences in participants having varying cognitive flexibility, we reported that in contrast to the low flexibility group, participants with high flexibility experienced extensively increased MCN connectivity and subsystem properties in the VN and SMN. These results consistently remind us that the intra- and inter-subsystem structural–functional coordination supports

Fig. 6. (Color online) The correlation between the actual and predicted TMT B–A scores. The colored circles denote the participants.

multiple cognitive functions, such as visuospatial search, motor, processing speed, etc., and the efficient MCN configuration will contribute highly to human cognitive flexibility. Moreover, MCN seems to be a reliable tool for future studies to disclose the structural–functional pre-configurations underlying human cognitive processes.

As an accessible neuropsychological test, the TMT has gained popularity for evaluating cognitive functions in individuals and identifying potential neuropsychological deficits.[13] The TMT can be conceptualized as a visuomotor sequence-tracking task, during which visual recognition and goal-directed, coordinated motor behavior are essential factors for accomplishing tasks.[60] The TMT B—A difference score, which is obtained by subtracting the completion time of TMT-B from that of TMT-A, is broadly acknowledged as a valid indicator of cognitive flexibility abilities.[15] In this study, we thus first reported significant relationships between the intra-subsystem covariation of the SMN/VN and TMT B–A scores (Fig. 1), highlighting their potential roles in responding to visuospatial search and motor demands.[14] Additionally, the parietal areas facilitate task completion by participating in the integration of visual information to regulate spatial movements[61,62]; the frontal activity has been shown to closely relate to the TMT for its involvement in executive functions, e.g. planning, processing speed, and attention.[63,64] Consequently, extensive inter-subsystem connectivity spanning the SMN and VN/FPN/DMN were identified to significantly correlate with the TMT B–A score. Overall, the
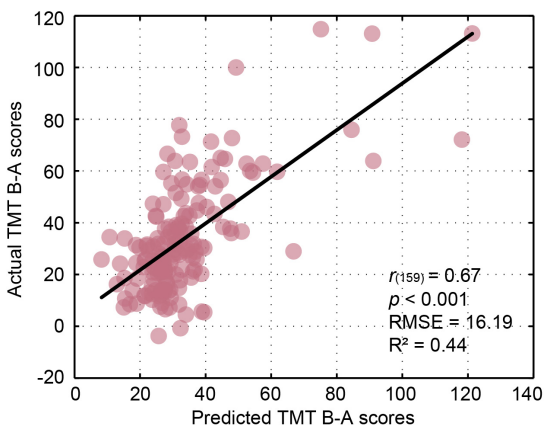
structural–functional coordination within and across subsystems at rest may establish the cognitive and attentional abilities required for the successful completion of the TMT task, thus supporting the brain's cognitive flexibility in processing task information efficiently.

Subsequently, we found that greater TMT B–A scores (indicating lower cognitive flexibility) corresponded to smaller Le, Ge, and C, as well as a longer L in Fig. 2, particularly in functional subsystems of SMN, VAN, and VN (Fig. 3 and Table 2). As proved, the increased Le, Ge, and C as well as the shorter L indicated an increase in the efficiency of information processing in the brain.[65] Here, the above results thereby reveal that participants with high-efficiency resting state MCN performed better in the TMT task. Previous research has indicated that the brain's activity at rest mirrors task-induced activity and can thus predict individual task behaviors,[66] an optimized brain organization concerning relevant resources at rest usually facilitates individual task behaviors, such as shorter reaction time[67] and larger component amplitude.[68] In general, TMT encompasses multifarious cognitive functions, e.g. psychomotor speed, sequencing and shifting, visual search and scanning, and attention,[69] the success in the TMT task will be attributed to the efficient integration and coordination of corresponding cognitive information that originates from the distributed regions. As such, the efficiently functioning brain (especially subsystems of the SMN, VAN, and VN) will then facilitate the higher cognitive processing related to the visuospatial materials, eventually contributing to a smaller TMT B–A score. In addition, the successful prediction of participants' TMT performance in Fig. 6 further confirmed the relevance of MCN as biomarkers of the cognitive flexibility of healthy participants.

Furthermore, considering the ability of MCN to reflect individual cognitive flexibility, we then explore the coordinated structural–functional organizations in participants with varying cognitive flexibility. As illustrated in Fig. 4(b), the high flexibility participants showed stronger intra-subsystem covariation in the VN and SMN and stronger inter-subsystem covarying spanning the VN and SMN/VAN/DAN. Owing to the visuomotor integration capabilities of the human brain, the VN

and SMN are strongly linked[70] And the increased inter-subsystem covarying with higher-level subsystems (i.e. VAN and DAN) are regarded as the marker that reflects the pre-configuration of attentional and working memory resources for the TMT task. And coinciding with the MCN topologies of the high flexibility participants, the efficient resting-state MCN pre-configuration was indeed quantified by the greater brain-wide Le, Ge, and C, as well as a smaller L, in Fig. 4(c), which was also the same for the subsystems of VN and SMN (Fig. 5 and Table 3). That is, for high flexibility participants, stronger intra- and inter-subsystem structural–functional interactions constitute the neurological foundation to accomplish the requested TMT tasks as accurately and quickly as possible, which also validated the negative relationship between the MCN and TMT B–A performance in Figs. 1–3.

Overall, our current work complements a previously unexplored issue regarding how structural–functional configurations support individual cognitive flexibility. Particularly in methodology, in comparison with previous studies that typically consider structural–functional organization at a group level,[23] individual-level MCN analyses were proposed and accomplished in our current study to capture the subject-specific structural–functional characteristics of each participant. This new strategy allows us to investigate potential structural–functional variation corresponding to inter-subject variability in cognitive flexibility, and exhibit superior sensitivity in reflecting human cognition compared to existing covariance networks.[24] Furthermore, it has the potential to tackle the "performance confounds" in the examination of cognitive impairment. Namely, any observed structural–functional alteration in people with cognitive impairment could be attributed as either a causal factor or an outcome of impaired cognitive task performance. Herein, the identification of resting-state markers may circumvent these confounding factors by enabling us to comprehend individual variations in cognitive flexibility based on independently estimated connectivity variables, irrespective of task performance.[71]

With the above strategies, our findings demonstrated that cognitive flexibility involves visual recognition and goal-directed, coordinated motor behavior that relies on the structural–functional

configuration among large-scale SMN, VN, and FPN enacting visuospatial search, attention, motor demands, processing speed, and spatial movement processes. In this regard, it is plausible to assume that patients with cognitive flexibility impairments may exhibit a decrease in the brain's structural–functional connections, especially for inter- and intra-subsystem structural–functional interactions among SMN, VN, and FPN. Understanding the typical progression and potential deterioration of these subsystems in connection with aging and pathology is essential as a preliminary measure towards recognizing efficient approaches for diagnosing and intervening flexibility deficiencies in neurological and psychiatric disorders, while simultaneously improving flexibility throughout all stages of life.[19] For instance, the discovery of unique brain structural–functional patterns that support different levels of flexibility among clinical and neurotypical groups may aid in identifying diagnostic and (drug) intervention markers with a higher likelihood of success for an individual. This will further contribute to enhancing current existing diagnostic nosology and advancing toward the objective of precision medicine.

Possible limitations should also be noticed in this study. On the one hand, the identified resting-state structural–functional circuit may not characterize the circuitry state when involved in the TMT task. Although our results may help to predict and evaluate cognitive flexibility performance in patients who cannot perform a given task (e.g. due to lack of consciousness), only behaviorally relevant resting-state circuits were insufficient to roundly characterize the brain's cognitive flexibility. In the future study, additional experiments including MRI-EEG recordings during the TMT task should be conducted to further validate and extend our findings. On the other hand, given our current findings were acquired based on correlation analysis, thus being incapable of reporting potential causal relationships between the MCN and individual cognitive flexibility, related intervention strategies, such as adopting transcranial magnetic stimulation, would be accomplished in the future to manipulate the brain's structural–functional configurations, in which related fluctuations of individual cognitive flexibility

would be accordingly explored, to mine if there exists any causal relationships between the two variables.

5. Conclusion

Herein, we performed MCN analyses to probe the correlation between cognitive flexibility and resting-state structural–functional coordination at the individual level. Results show that structural–functional MCN plays an essential role in cognitive flexibility, and individuals with efficient resting-state brain pre-configurations tend to perform better during the TMT task and achieve a relatively small TMT B–A score. Further analysis confirmed that the resting-state MCN features can effectively predict an individual's TMT task performance. Collectively, current discoveries enhanced our understanding of cognitive flexibility from the viewpoint of structural–functional interaction and will further derive useful physiological markers of cognitive functioning.

Data and Code Availability

The multimodal datasets used in this work can be found at the Functional Connectomes Project International Neuroimaging Data-Sharing Initiative http://doi.org/10.15387/fcp_indi.mpi_lemon (2018).[28] The MRI datasets are processed by Free-Surfer v6.0 (http://surfer.nmr.mgh.harvard.edu/), FSL v6.0 (https://fsl.fmrib.ox.ac.uk/fsl/fslwiki), and DPABI v7.0 (http://rfmri.org/DPABI). The EEG pre-processing toolboxes are freely available (EEGLAB v2020.0, https://sccn.ucsd.edu/eeglab/index.php, and REST_v1.2_20200818, https://github.com/webrain2018/REST). The codes for MCN construction and the following analysis are available at https://github.com/yangnvmumu/MCN_SourceCode. Large-scale MCN properties were

computed by the Brain Connectivity Toolbox (www.nitrc.org/projects/bct/). The visualization of sub-network distribution images was conducted using BrainNetViewer 1.7 (https://www.nitrc.org/projects/bnv/). The statistical visualization of TMT B–A scores and network properties was conducted using GraphPad Prism 8.3 (https://www.graphpad.com/).

ORCID

Lin Jiang https://orcid.org/0000-0002-7892-118X

Simon B. Eickhoff https://orcid.org/0000-0001-6363-2759

Sarah Genon https://orcid.org/0000-0002-7087-7882

Guangying Wang https://orcid.org/0000-0002-6622-3157

Chanlin Yi https://orcid.org/0000-0001-7989-2440

Runyang He https://orcid.org/0009-0008-0378-8995

Xunan Huang https://orcid.org/0000-0002-1474-4225

Dezhong Yao https://orcid.org/0000-0002-8042-879X

Debo Dong https://orcid.org/0000-0002-8931-2806

Fali Li https://orcid.org/0000-0002-2450-4591

Peng Xu https://orcid.org/0009-0004-6198-8195

References

1. R. Spiro, P. J. Feltovich, M. Jacobson and R. Coulson, Cognitive flexibility, constructivism, and hypertext: Random access instruction for advanced knowledge acquisition in ILL-structured domains, *Educ. Technol. Soc.* **31**(5) (1991) 24–33.

2. R. L. Coulson, P. J. Feltovich and R. J. Spiro, Cognitive flexibility in medicine: An application to the recognition and understanding of hypertension, *Adv. Health Sci. Educ.* **2**(2) (1997) 141–161.

3. R. Spiro, P. J. Feltovich, M. Jacobson and R. Coulson, *Constructivism and the Technology of Instruction* (Routledge, New York, 2013).

4. S. Braem and T. Egner, Getting a grip on cognitive flexibility, *Curr. Dir. Psychol.* **27**(6) (2018) 470–476.

5. F. Roshani, R. Piri, A. Malek, T. M. Michel and M. S. Vafaee, Comparison of cognitive flexibility, appropriate risk-taking and reaction time in individuals with and without adult ADHD, *Psychiatry Res.* **284** (2020) 112494.

6. F. Lange, C. Seer, S. Loens, F. Wegner, C. Schrader, D. Dressler, R. Dengler and B. Kopp, Neural mechanisms underlying cognitive inflexibility in Parkinson's disease, *Neuropsychologia* **93** (2016) 142–150.

7. H. M. Geurts, B. Corbett and M. Solomon, The paradox of cognitive flexibility in autism, *Trends Cogn. Sci.* **13**(2) (2009) 74–82.

8. Z. Ben-Zion, N. B. Fine, N. J. Keynan, R. Admon, N. Green, M. Halevi, G. A. Fonzo, M. Achituv, O. Merin, H. Sharon, P. Halpern, I. Liberzon, A. Etkin, T. Hendler and A. Y. Shalev, Cognitive flexibility predicts PTSD symptoms: Observational and interventional studies, *Front. Psychiatry* **9** (2018) 477.

9. B. Lee, W. Cai, C. B. Young, R. Yuan, S. Ryman, J. Kim, V. Santini, V. W. Henderson, K. L. Poston and V. Menon, Latent brain state dynamics and cognitive flexibility in older adults, *Prog. Neurobiol.* **208** (2022) 102180.

10. C. Porcaro, F. Vecchio, F. Miraglia, G. Zito and P. M. Rossini, Dynamics of the "cognitive" brain wave P3b at rest for Alzheimer dementia prediction in mild cognitive impairment, *Int. J. Neural Syst.* **32**(05) (2022) 2250022.

11. C. Jiménez-Mesa, J. E. Arco, M. Valentí-Soler, B. Frades-Payo, M. A. Zea-Sevilla, A. Ortiz, M. Ávila-Villanueva, D. Castillo-Barnes, J. Ramírez, T. D. Ser-Quijano, C. Carnero-Pardo and J. M. Górriz, Using explainable artificial intelligence in the clock drawing test to reveal the cognitive impairment pattern, *Int. J. Neural Syst.* **33**(04) (2023) 2350015.

12. P. Singh, M. Wtorek, A. Ceglarek, M. Fąfrowicz, K. Lewandowska, T. Marek, B. Sikora-Wachowicz and P. Oświęcimka, Analysis of fMRI signals from working memory tasks and resting-state of brain: Neutrosophic-entropy-based clustering algorithm, *Int. J. Neural Syst.* **32**(04) (2022) 2250012.

13. C. R. Bowie and P. D. Harvey, Administration and interpretation of the trail making test, *Nat. Protoc.* **1**(5) (2006) 2277–2281.

14. A. Varjacic, D. Mantini, N. Demeyere and C. R. Gillebert, Neural signatures of Trail Making Test performance: Evidence from lesion-mapping and neuroimaging studies, *Neuropsychologia* **115** (2018) 78–87.

15. I. Sánchez-Cubillo, J. A. Periáñez, D. Adrover-Roig, J. M. Rodríguez-Sánchez, M. Ríos-Lago, J. Tirapu and F. Barceló, Construct validity of the Trail Making Test: Role of task-switching, working memory, inhibition/interference control, and visuomotor abilities, *J. Int. Neuropsychol. Soc.* **15**(3) (2009) 438–450.

16. M. R. van Schouwenburg, J. O'Shea, R. B. Mars, M. F. S. Rushworth and R. Cools, Controlling human striatal cognitive function via the frontal cortex, *J. Neurosci.* **32**(16) (2012) 5631–5637.

17. J. Zhu, D. Zhu, C. Zhang, Y. Wang, Y. Yang and Y. Yu, Quantitative prediction of individual cognitive flexibility using structural MRI, *Brain Imaging Behav.* **13** (2019) 781–788.

18. A. K. Barbey, R. Colom and J. Grafman, Architecture of cognitive flexibility revealed by lesion mapping, *Neuroimage* **82** (2013) 547–554.

19. L. Q. Uddin, Cognitive and behavioural flexibility: Neural mechanisms and clinical considerations, *Nat. Rev. Neurosci.* **22**(3) (2021) 167–179.

20. D. R. Dajani and L. Q. Uddin, Demystifying cognitive flexibility: Implications for clinical and developmental neuroscience, *Trends Neurosci.* **38**(9) (2015) 571–578.

21. N. G. Harnett, J. S. Stevens, N. Fani, S. J. H. van Rooij, T. D. Ely, V. Michopoulos, L. Hudak, A. O. Rothbaum, R. Hinrichs, S. J. Winters, T. Jovanovic, B. O. Rothbaum, L. D. Nickerson and K. J. Ressler, Acute posttraumatic symptoms are associated with multimodal neuroimaging structural covariance patterns: A possible role for the neural substrates of visual processing in posttraumatic stress disorder, *Biol. Psychiatry:Cogn. Neurosci. Neuroimaging* **7**(2) (2022) 129–138.

22. G. Deco, M. L. Kringelbach, A. Arnatkeviciute, S. Oldham, K. Sabaroedin, N. C. Rogasch, K. M. Aquino and A. Fornito, Dynamical consequences of regional heterogeneity in the brain's transcriptional landscape, *Sci. Adv.* **7**(29) (2021) eabf4752.

23. L. Jiang, F. Li, B. Chen, C. Yi, Y. Peng, T. Zhang, D. Yao and P. Xu, The task-dependent modular covariance networks unveiled by multiple-way fusion-based analysis, *Int. J. Neural Syst.* **32**(07) (2022) 2250035.

24. L. Jiang, Y. Peng, R. He, Q. Yang, C. Yi, Y. Li, B. Zhu, Y. Si, T. Zhang, B. B. Biswal, D. Yao, L. Xiong, F. Li and P. Xu, Transcriptomic and macroscopic architectures of multimodal covariance network reveal molecular–structural–functional co-alterations, *Research* **6** (2023) 0171.

25. C. Chang and J. E. Chen, Multimodal EEG-fMRI: Advancing insight into large-scale human brain dynamics, *Curr. Opin. Biomed. Eng.* **18** (2021) 100279.

26. R. Yuvaraj, M. Murugappan, U. R. Acharya, H. Adeli, N. M. Ibrahim and E. Mesquita, Brain functional connectivity patterns for emotional state classification in Parkinson's disease patients without dementia, *Behav. Brain Res.* **298** (2016) 248–260.

27. J. D. Medaglia, W. Huang, E. A. Karuza, A. Kelkar, S. L. Thompson-Schill, A. Ribeiro and D. S. Bassett, Functional alignment with anatomical networks is associated with cognitive flexibility, *Nat. Hum. Behav.* **2**(2) (2018) 156–164.

28. A. Babayan, M. Erbey, D. Kumral, J. D. Reinelt, A. M. F. Reiter, J. Röbbig, H. L. Schaare, M. Uhlig, A. Anwander and P.-L. Bazin, A mind-brain-body dataset of MRI, EEG, cognition, emotion, and peripheral physiology in young and old adults, *Sci. Data* **6**(1) (2019) 1–21.

29. T. N. Tombaugh, Trail making test A and B: Normative data stratified by age and education, *Arch. Clin. Neuropsychol.* **19**(2) (2004) 203–214.

30. M. Jenkinson, C. F. Beckmann, T. E. Behrens, M. W. Woolrich and S. M. Smith, FSL, *Neuroimage* **62**(2) (2012) 782–790.

31. N. Mendes, S. Oligschläger, M. E. Lauckner, J. Golchert, J. M. Huntenburg, M. Falkiewicz, M. Ellamil, S. Krause, B. M. Baczkowski, R. Cozatl, A. Osoianu, D. Kumral, J. Pool, L. Golz, M. Dreyer, P. Haueis, R. Jost, Y. Kramarenko, H. Engen, K. Ohrnberger, K. J. Gorgolewski, N. Farrugia, A. Babayan, A. Reiter, H. L. Schaare, J. Reinelt, J. Röbbig, M. Uhlig, M. Erbey, M. Gaebler, J. Smallwood, A. Villringer and D. S. Margulies, A functional connectome phenotyping dataset including cognitive state and personality measures, *Sci. Data* **6**(1) (2019) 180307.

32. P. L. Bazin, M. Weiss, J. Dinse, A. Schäfer, R. Trampel and R. Turner, A computational framework for ultra-high resolution cortical segmentation at 7 Tesla, *Neuroimage* **93** (2014) 201–209.

33. A. M. Dale, B. Fischl and M. I. Sereno, Cortical surface-based analysis: I. Segmentation and surface reconstruction, *Neuroimage* **9**(2) (1999) 179–194.

34. G. Mirzaei and H. Adeli, Segmentation and clustering in brain MRI imaging, *Rev. Neurosci.* **30**(1) (2018) 31–44.

35. B. B. Avants, C. L. Epstein, M. Grossman and J. C. Gee, Symmetric diffeomorphic image registration with cross-correlation: Evaluating automated labeling of elderly and neurodegenerative brain, *Med. Image Anal.* **12**(1) (2008) 26–41.

36. B. B. Avants, N. J. Tustison, G. Song, P. A. Cook, A. Klein and J. C. Gee, A reproducible evaluation of ANTs similarity metric performance in brain image registration, *Neuroimage* **54**(3) (2011) 2033–2044.

37. D. Yao, A method to standardize a reference of scalp EEG recordings to a point at infinity, *Physiol. Meas.* **22**(4) (2001) 693.

38. T. He, G. Clifford and L. Tarassenko, Application of independent component analysis in removing artefacts from the electrocardiogram, *Neural Comput. Appl.* **15**(2) (2006) 105–116.

39. R. D. Pascual-Marqui, Standardized low resolution brain electromagnetic tomography (SLORETA): Technical details, *Methods Find. Exp. Clin. Pharmacol.* **24**(Suppl D) (2002) 5–12.

40. S. E. Morgan, J. Seidlitz, K. J. Whitaker, R. Romero-Garcia, N. E. Clifton, C. Scarpazza, T. van Amelsvoort, M. Marcelis, J. van Os and G. Donohoe, Cortical patterning of abnormal morphometric similarity in psychosis is associated with brain expression of schizophrenia-related genes, *Proc. Natl. Acad. Sci. USA* **116**(19) (2019) 9604–9609.

41. S. N. Vandekar, R. T. Shinohara, A. Raznahan, R. D. Hopson, D. R. Roalf, K. Ruparel, R. C. Gur, R. E. Gur and T. D. Satterthwaite, Subject-level measurement of local cortical coupling, *Neuroimage* **133** (2016) 88–97.

42. K. J. Whitaker, P. E. Vértes, R. Romero, F. Váša, M. Moutoussis, G. Prabhu, N. Weiskopf, M. F. Callaghan, K. Wagstyl, and T. Rittman, Adolescence is associated with genomically patterned consolidation of the hubs of the human brain connectome, *Proc. Natl. Acad. Sci. USA* **113**(32) (2016) 9105–9110.

43. M. R. Sabuncu, T. Ge, A. J. Holmes, J. W. Smoller, R. L. Buckner, B. Fischl and I. Alzheimer's, Disease Neuroimaging, Morphometricity as a measure of the neuroanatomical signature of a trait, *Proc. Natl. Acad. Sci. USA* **113**(39) (2016) E5749–E5756.

44. K. A. Clark, K. H. Nuechterlein, R. F. Asarnow, L. S. Hamilton, O. R. Phillips, N. S. Hageman, R. P. Woods, J. R. Alger, A. W. Toga and K. L. Narr, Mean diffusivity and fractional anisotropy as indicators of disease and genetic liability to schizophrenia, *J. Psychiatr. Res.* **45**(7) (2011) 980–988.

45. X. Long, W. Liao, C. Jiang, D. Liang, B. Qiu and L. Zhang, Healthy aging: An automatic analysis of global and regional morphological alterations of human brain, *Acad. Radiol.* **19**(7) (2012) 785–793.

46. J. S. Shimony, C. D. Smyser, G. Wideman, D. Alexopoulos, J. Hill, J. Harwell, D. Dierker, D. C. Van Essen, T. E. Inder and J. J. Neil, Comparison of cortical folding measures for evaluation of developing human brain, *Neuroimage* **125** (2016) 780–790.

47. Y. F. Zang, Y. He, C. Z. Zhu, Q. J. Cao, M. Q. Sui, M. Liang, L. X. Tian, T. Z. Jiang and Y. F. Wang, Altered baseline brain activity in children with ADHD revealed by resting-state functional MRI, *Brain Dev.* **29**(2) (2007) 83–91.

48. A. P. A. Bueno, W. H. L. Pinaya, K. Rebello, L. C. de Souza, M. Hornberger and J. R. Sato, Regional dynamics of the resting brain in amyotrophic lateral sclerosis using fractional amplitude of low-frequency fluctuations and regional homogeneity analyses, *Brain Connect.* **9**(4) (2019) 356–364.

49. S. Wainio-Theberge, A. Wolff and G. Northoff, Dynamic relationships between spontaneous and evoked electrophysiological activity, *Commun. Biol.* **4**(1) (2021) 741.

50. M. Rubinov and O. Sporns, Complex network measures of brain connectivity: Uses and interpretations, *Neuroimage* **52**(3) (2010) 1059–1069.

51. M. Ahmadlou and H. Adeli, Complexity of weighted graph: A new technique to investigate structural complexity of brain activities with applications to aging and autism, *Neurosci. Lett.* **650** (2017) 103–108.

52. J. delEtoile and H. Adeli, Graph theory and brain connectivity in Alzheimer's disease, *Neuroscientist* **23**(6) (2017) 616–626.

53. L. Jiang, Y. Liang, S. Genon, R. He, Q. Yang, C. Yi, L. Yu, D. Yao, S. B. Eickhoff and D. Dong, Spatial–rhythmic network as a biomarker of familial risk for psychotic bipolar disorder, *Nat. Mental Health* **1** (2023) 1–13.

54. F. Li, Q. Tao, W. Peng, T. Zhang, Y. Si, Y. Zhang, C. Yi, B. Biswal, D. Yao and P. Xu, Inter-subject P300 variability relates to the efficiency of brain networks reconfigured from resting-to task-state: Evidence from a simultaneous event-related EEG-fMRI study, *Neuroimage* **205** (2020) 116285.

55. S. Goyal, V. V. Patage and S. Tiwari, Gender and age group predictions from speech features using multilayer perceptron model, in *2020 IEEE 17th India Council Int. Conf. (INDICON)* (IEEE, New Delhi, India, 2020), pp. 1–6.

56. L. Jiang, F. Li, Z. Chen, B. Zhu, C. Yi, Y. Li, T. Zhang, Y. Peng, Y. Si and Z. Cao, Information transmission velocity-based dynamic hierarchical brain networks, *Neuroimage* **270** (2023) 119997.

57. D. Chicco, M. J. Warrens and G. Jurman, The coefficient of determination R-squared is more informative than SMAPE, MAE, MAPE, MSE and RMSE in regression analysis evaluation, *PeerJ Comput. Sci.* **7** (2021) e623.

58. T. Ionescu, Exploring the nature of cognitive flexibility, *New Ideas Psychol.* **30**(2) (2012) 190–200.

59. B. T. Yeo, F. M. Krienen, J. Sepulcre, M. R. Sabuncu, D. Lashkari, M. Hollinshead, J. L. Roffman, J. W. Smoller, L. Zöllei and J. R. Polimeni, The organization of the human cerebral cortex estimated by intrinsic functional connectivity, *J. Neurophysiol.* **106**(3) (2011) 1125–1165.

60. J. M. Schear and S. D. Sato, Effects of visual acuity and visual motor speed and dexterity on cognitive test performance, *Arch. Clin. Neuropsychol.* **4**(1) (1989) 25–32.

61. J. C. Culham, C. Cavina-Pratesi and A. Singhal, The role of parietal cortex in visuomotor control: What have we learned from neuroimaging? *Neuropsychologia* **44**(13) (2006) 2668–2684.

62. M. Husain and P. Nachev, Space and the parietal cortex, *Trends Cogn. Sci.* **11**(1) (2007) 30–36.

63. K. Hagen, A.-C. Ehlis, F. B. Haeussinger, S. Heinzel, T. Dresler, L. D. Mueller, M. J. Herrmann, A. J. Fallgatter and F. G. Metzger, Activation during the trail making test measured with functional near-infrared spectroscopy in healthy elderly subjects, *Neuroimage* **85** (2014) 583–591.

64. L. D. Müller, A. Guhn, J. B. M. Zeller, S. C. Biehl, T. Dresler, T. Hahn, A. J. Fallgatter, T. Polak, J. Deckert and M. J. Herrmann, Neural correlates of a standardized version of the trail making test in young and elderly adults: A functional near-infrared spectroscopy study, *Neuropsychologia* **56** (2014) 271–279.

65. Y. Si, L. Jiang, Q. Tao, C. Chen, F. Li, Y. Jiang, T. Zhang, X. Cao, F. Wan, D. Yao and P. Xu, Predicting individual decision-making responses based on the functional connectivity of resting-state EEG, *J. Neural Eng.* **16**(6) (2019) 066025.

66. A. H. C. Fong, K. Yoo, M. D. Rosenberg, S. Zhang, C. R. Li, D. Scheinost, R. T. Constable and M. M. Chun, Dynamic functional connectivity during task performance and rest predicts individual differences in attention across studies, *Neuroimage* **188** (2019) 14–25.

67. G. Zhou, P. Liu, J. He, M. Dong, X. Yang, B. Hou, K. Von Deneen, W. Qin and J. Tian, Interindividual

reaction time variability is related to resting-state network topology: An electroencephalogram study, *Neuroscience* **202** (2012) 276–282.

68. F. Li, T. Liu, F. Wang, H. Li, D. Gong, R. Zhang, Y. Jiang, Y. Tian, D. Guo and D. Yao, Relationships between the resting-state network and the P3: Evidence from a scalp EEG study, *Sci. Rep.* **5** (2015) 15129.

69. T. A. Salthouse, What cognitive abilities are involved in trail-making performance? *Intelligence* **39**(4) (2011) 222–232.

70. M. A. Goodale, Transforming vision into action, *Vision Res.* **51**(13) (2011) 1567–1587.

71. Q. Zou, T. J. Ross, H. Gu, X. Geng, X. N. Zuo, L. E. Hong, J. H. Gao, E. A. Stein, Y. F. Zang and Y. Yang, Intrinsic resting-state activity predicts working memory brain activation and behavioral performance, *Hum. Brain Mapp.* **34**(12) (2013) 3204–3215.